JACS
JOURNAL OF THE AMERICAN CHEMICAL SOCIETY
pubs.acs.org/JACS
Article

Probing Lanmodulin's Lanthanide Recognition via Sensitized Luminescence Yields a Platform for Quantification of Terbium in Acid Mine Drainage

Emily R. Featherston, Edward J. Issertell, and Joseph A. Cotruvo, Jr.*

Cite This: https://doi.org/10.1021/jacs.1c06360
Read Online

ABSTRACT: Lanmodulin is the first natural, selective macrochelator for f elements—a protein that binds lanthanides with picomolar affinity at 3 EF hands, motifs that instead bind calcium in most other proteins. Here, we use sensitized terbium luminescence to probe the mechanism of lanthanide recognition by this protein as well as to develop a terbium-specific biosensor that can be applied directly in environmental samples. By incorporating tryptophan residues into specific EF hands, we infer the order of metal binding of these three sites. Despite lanmodulin's remarkable lanthanide binding properties, its coordination of approximately two solvent molecules per site (by luminescence lifetime) and metal dissociation kinetics (k_{off} = 0.02−0.05 s^{-1}, by stopped-flow fluorescence) are revealed to be rather ordinary among EF hands; what sets lanmodulin apart is that metal association is nearly diffusion limited ($k_{on} \approx 10^9$ M^{-1} s^{-1}). Finally, we show that Trp-substituted lanmodulin can quantify 3 ppb (18 nM) terbium directly in acid mine drainage at pH 3.2 in the presence of a 100-fold excess of other rare earths and a 100 000-fold excess of other metals using a plate reader. These studies not only yield insight into lanmodulin's mechanism of lanthanide recognition and the structures of its metal binding sites but also show that this protein's unique combination of affinity and selectivity outperforms synthetic luminescence-based sensors, opening the door to rapid and inexpensive methods for selective sensing of individual lanthanides in the environment and in-line monitoring in industrial operations.

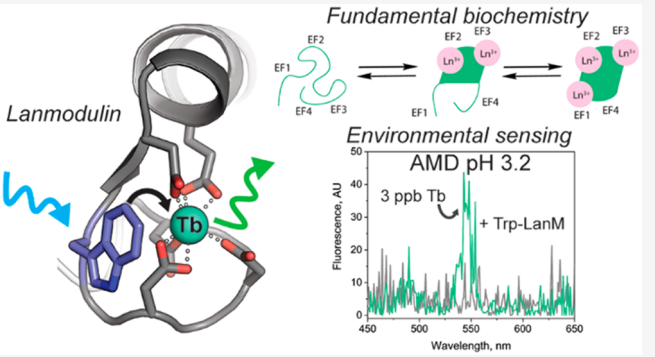

INTRODUCTION

The rare earth elements (REEs)—a family of elements comprised of the 15 lanthanides plus yttrium and scandium—possess similar physicochemical properties and play indispensable roles in the emerging green economy.[1] With increasing technological dependence on these elements, however, the chemical, environmental, and political challenges associated with mining and processing REEs have been magnified.[2−4] These complexities have driven interest in obtaining REEs more sustainably from low-grade but abundant nontraditional sources, such as coal byproducts, mine effluents [e.g., acid mine drainage (AMD)], and recycling from electronic waste (E-waste).[5,6] The discovery that biology is able to selectively recognize and utilize the lighter lanthanides, especially La−Nd,[7−12] offers new possibilities for efficient biotechnologies to meet these challenges.[13] This promise has been accelerated with the recent identification of the first native, selective biological chelator for the lanthanides, lanmodulin (LanM).[14] This small (12-kDa) protein undergoes a conformational change that is 10^8-fold more selective for lanthanides (with a preference for the lighter REEs) over non-REEs tested to date.[14,15] The protein tolerates acidic conditions (pH < 2) relevant to environmental REE streams and industrial processes, and it is able to quantitatively extract REEs from acidic coal and E-waste leachates with high purity, outperforming traditional chelators.[15] From a chemical perspective, this selectivity for REEs is all the more remarkable because the protein utilizes EF hands, carboxylate-rich metal binding motifs associated with Ca^{II} recognition in most of the hundreds of other characterized examples.[16,17] An understanding of the fundamentals underlying LanM's selective recognition of REEs may translate not only to more efficient approaches for REE extraction and separations but also to simpler and portable methods of REE detection (also necessary for ensuring a sustainable supply of REEs), as we demonstrate in the present work.

Received: June 20, 2021

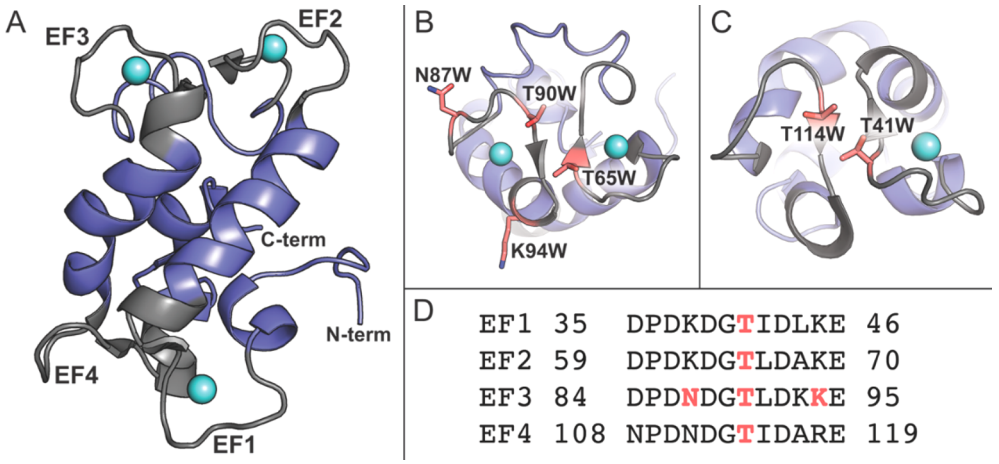

Figure 1. (A) NMR solution structure of Y^{III}-bound LanM, highlighting EF hands 1−4 in gray, with Y^{III} ions shown as cyan spheres.[18] (B) Pairing of EF2 (right) and EF3 (left), indicating sites of individual Trp substitutions in salmon sticks, at EF3 positions N87, T90, and K94 and EF2 position T65. (C) Individual Trp substitutions in EF4 at position T114 (left) and EF1 at position T41 (right) indicated by salmon sticks. (D) Sequences of the EF hands of LanM, highlighting the positions at which Trp residues were substituted in this work in salmon.

Biochemical characterization of *Methylorubrum extorquens* LanM[14] suggested that binding of REEs to two of the protein's three metal-binding sites occurs cooperatively with a picomolar apparent K_d, inducing formation of two-thirds of the protein's helical content; a third site binds with similar but slightly weaker affinity, contributing the remaining one-third. The NMR structure of lanmodulin, obtained in the presence of the diamagnetic Y^{III} ion, revealed the overall structure of the protein, the three REE-binding EF hands (EF1−3), and a hydrophobic core that may help stabilize the REE-bound state of the protein (Figure 1), but it left many questions unanswered.[18] Although the protein architecture is unusual for an EF-hand protein, the pairing of EF2 and EF3 suggested that they might account for the cooperative metal binding phase. Alternatively, the unusual connection of EF1 and EF2 through a single, short α-helix made stabilization of this helix via cooperative metal binding to EF1 and EF2 also a plausible source of the cooperative phase (Figure S1). Furthermore, the detailed structure of the sites—in particular, whether solvent molecules contributed to the coordination spheres of the metal ions—could not be determined from the NMR structure. Therefore, the means by which the structural and kinetic properties of the metal sites contribute to LanM's unique REE affinity and selectivity still remain to be determined.

In order to answer these questions, it is necessary to probe each metal binding site specifically. Several lanthanide(III) ions (Ln^{III}) display intrinsic luminescence with relatively long luminescence lifetimes, especially in the cases of Tb^{III} and Eu^{III}, and diagnostic emission spectra.[19] Lanthanide f−f transitions are Laporte forbidden, and therefore, direct excitation is inefficient; this limitation can be overcome by incorporating a photosensitizer adjacent to the metal ion to absorb and transfer energy to the metal ion excited state (luminescence resonance energy transfer, LRET).[20−24] The requirement for a nearby sensitizer is advantageous in that it enables probing of individual metal binding sites utilizing chromophores (e.g., tyrosine or tryptophan) in the protein, either native or incorporated via site-directed mutagenesis.[25,26] This strategy has been employed extensively in proteins for characterization of metal binding affinity,[27] deduction of binding order and metal−metal distances in multimetallic systems,[28−30] dissociation kinetics,[31−33] and solvent coordination,[34] especially in Ca^{II} binding EF-hand proteins, due to similarities in ionic radius and coordination preferences of Ca^{II} and Ln^{III} ions, such as Tb^{III}. However, this method has yet to be applied to understand a natural, dedicated lanthanide-binding biomolecule.

In addition to their utility in biology and as biochemical probes, sensitive methods for detection of REEs are essential both in the identification of potential sources for REE recovery and in monitoring of industrial REE processing operations. Inductively coupled plasma mass spectrometry (ICP-MS) is the gold-standard method but expensive and not portable, whereas portable instruments like X-ray fluorescence spectrometers are limited by interferences and low sensitivity.[35,36] As recently comprehensively reviewed,[37] luminescence-based methods are attractive alternatives, especially in the case of Tb^{III}, which is both readily sensitized and one of the rarest and most valuable REEs.[38] Terbium is one of five REEs deemed by the United States as the most economically critical, for its utility including in phosphors in energy-efficient lighting[39] as well as for its domestic supply risk.[40] Despite recent progress to decrease limits of detection (LODs) for Tb^{III} even at low pH and in AMD matrix,[41,42] popular approaches utilizing small molecules or metal−organic frameworks (MOFs) still lack the necessary selectivity, requiring spiking of samples with Tb^{III} for detection. By contrast, biomolecular luminescence-based sensors for Tb^{III} based on Trp-containing EF hands such as lanthanide binding tags (LBTs) exhibit better selectivity, but their affinities ($K_d \approx 50$ nM[43,44] or weaker[45] at pH 7) are insufficient for applications below pH ≈ 6.[46] As a step toward more sensitive detection of REEs, our laboratory recently reported a selective FRET-based sensor for REEs (LaMP1), taking advantage of LanM's large conformational response.[47] LaMP1 facilitated discovery of key elements of lanthanide uptake machinery in bacteria, but its use is limited to near-neutral pH values, it cannot distinguish between REEs, and it exhibits a small but significant response to some non-REEs at high concentrations. Consequently, it is unsuitable for complex environmental samples. We hypothesized that the combination of LanM's high affinity and selectivity for lanthanides with sensitized luminescence might allow for efficient and specific detection of terbium. However, low-grade natural sources of REEs like AMD are acidic and contain very low REE

https://doi.org/10.1021/jacs.1c06360
J. Am. Chem. Soc. XXXX, XXX, XXX−XXX

concentrations, <1 ppm, and Tb^{III} at parts per billion levels (1 ppb $Tb^{III} \approx 6$ nM).[6] Indeed, to the best of our knowledge, no luminescence-based sensors have been successfully deployed to quantify, or even detect, terbium at natural levels in these matrices.

Here, we show how strategic insertion of tryptophan residues into lanmodulin enables definition of key aspects of the protein's selective REE recognition, including metal site-specific thermodynamics, kinetics, and structure. These insights also suggest how the protein might be optimized further for biotechnological applications. Furthermore, we show that one of these Trp-LanM variants enables detection and quantification of Tb^{III} levels directly in AMD, a challenging matrix inaccessible to previously characterized luminescent sensors. Together, our work suggests that this technology could be extended for detection of other luminescent f elements and that LanM might enable harvesting of REEs from AMD.

EXPERIMENTAL SECTION

General Considerations. Terbium(III) chloride hexahydrate (99.9%) and general laboratory chemicals for protein expression and purification and buffer preparation were obtained from Millipore Sigma. Deuterium oxide (99.9%) was purchased from Cambridge Isotope Laboratories. Primers were ordered from Integrated DNA Technologies (IDT). *E. coli* strains [5alpha and BL21(DE3)] for cloning and recombinant protein expression, respectively, as well as cloning reagents (Q5 DNA polymerase, OneTaq Quick-Load, KLD Enzyme Mix, DpnI) were purchased from New England Biolabs. Miniprep kits were from Omega Biotek. Protein gel electrophoresis was carried out using Invitrogen Novex WedgeWell 16% Tris-Glycine gels and a mini gel apparatus. Chelex 100 resin was purchased from BioRad. Automated protein chromatography was carried out on a GE Healthcare Biosciences Äkta Pure fast protein liquid chromatography (FPLC) system. UV−vis absorption spectra were obtained on an Agilent Cary 60 UV−visible spectrophotometer using a quartz cuvette (Starna Cells). Well plates were analyzed using a BioTek Synergy H1 microplate reader. Fluorescence titrations and lifetime determinations were carried out on Cary Eclipse and PerkinElmer FL6500 spectrofluorometers, respectively, using a quartz septum cell microfluorometer cuvette (10 mm path length, Starna Cells). Circular dichroism measurements were carried out in the X-ray Crystallography and Automated Biological Calorimetry Facility at Penn State using a 1 mm path length quartz CD cuvette (Jasco J/0556). Stopped-flow UV−vis measurements were made on an Applied Photophysics SX20 spectrophotometer equipped with a 450 long-pass filter (Corion LL-450-F-T539) and a fluorescence detector. All protein and metal solutions were made in 2 mL microcentrifuge tubes or 15 or 50 mL centrifuge tubes purchased from Sarstedt. All thermodynamic and kinetic data were analyzed, and curve fitting was performed, in Origin 2018.

Acid Mine Drainage (AMD). The AMD sample was collected from the feed of an AMD treatment facility operated by the Pennsylvania Department of Environmental Protection (Pennsylvania, United States). The source—the same as that used recently by Pisupati and co-workers,[6] albeit collected at a different time—was from the lower Kittanning coal seam. The metal content of the sample was analyzed using inductively coupled plasma mass spectrometry (ICP-MS) on a Thermo Fisher Scientific ICAP RQ ICP-MS instrument at the Penn State College of Earth and Mineral Sciences, Earth and Environmental Systems Institute, Laboratory for Isotopes and Metals in the Environment. The AMD sample was diluted 20× into 2% HNO_3 (Aristar Ultra, BDH VWR Analytical), and a blank of 2% HNO_3 was subtracted from each analyte prior to elemental content determination. The pH of the sample was 3.24.

Construction, Expression, and Purification of Trp-Substituted LanM (Trp-LanM) Variants. Mutagenesis of T41, T65, N87, T90, K94, and T114 to W was performed on pET24a-LanM using the forward and reverse primers shown in Table S1 using NEB KLD enzyme mix. Reactions were run for 4 h at room temperature and then supplemented with 2 U/μL DpnI for 30 min at 37 °C prior to transformation. Transformants were screened for insert by colony PCR (OneTaq Quick-Load), and the correct insert was confirmed by DNA sequencing by Genewiz, yielding the plasmids in Table S2. The variants were expressed and purified as described for the wild-type (wt) protein and stored in 20 mM MOPS, 100 mM KCl, 5 mM acetate, 5% glycerol, pH 7.0 (Buffer A).[48]

Determination of Optimal Trp Insertion Points for LRET. Initial screening for the most suitable positions for Trp placement within LanM's EF hands utilized the EF3 Trp-substituted variants, N87W, T90W, and K94W. Stoichiometric LRET titrations of 20 μM protein in 20 mM MOPS, 100 mM KCl, 5 mM acetate, pH 7.0 (Buffer B) were carried out with a 2 mM solution of $TbCl_3$ in the same buffer. Titrations were performed on a Cary Eclipse fluorescence spectrophotometer using a 10 mm path length quartz septum cell microfluorometer cuvette (Starna Cells) with the following instrument parameters: 280 nm excitation, 400−700 nm emission scan, 5 nm excitation and emission slit widths, 120 nm/min scan rate, 1 nm data interval, 250−395 nm excitation filter, 430−1100 nm emission filter, and high PMT voltage setting. A blank solution of buffer was subtracted from each spectrum prior to analysis, and spectra were corrected for volume change prior to plotting. Substituting the seventh position in EF3 (T90W) revealed the greatest magnitude of LRET signal at 545 nm (Figure S2), and this position was selected as the optimal position for Trp substitutions in each EF hand (T41W, T65W, T90W, T114W) from the perspective of signal intensity.

Circular Dichroism Spectroscopy on wt LanM and Trp-LanM Variants. Circular dichroism (CD) spectra of wt LanM and Trp-LanM variants were collected using a Jasco J-1500 CD spectrometer, thermostated at 25 °C, using a 1 mm path length quartz CD cuvette. Samples were scanned from 260 to 190 nm with the following instrument settings: 1.00 nm bandwidth, 0.5 nm data pitch, 50 nm/min scan rate, 4 s average time. The cuvette contained 15 μM protein in 200 μL of Chelex-treated 30 mM MOPS, 100 mM KCl, pH 7.2 (Buffer C), into which 1−5 of equiv $TbCl_3$ was titrated, and spectra were acquired. Three scans were acquired and averaged for each condition. A buffer blank spectrum was subtracted from each sample spectrum, and the spectra were corrected for volume change before plotting.

K_d Determinations Using CD Spectroscopy. Solutions of Tb^{III} with free metal concentration buffered using ethylenediamine *N*,*N*′-disuccinic acid (EDDS), a chelator well matched with LanM's lanthanide affinity, were prepared as described, in Buffer C.[14] Protein was added to the low and high Tb^{III}−EDDS solutions separately to a final concentration of 15 μM, and EDDS solutions were mixed at various high:low ratios. The same ratio of high:low solutions was prepared without protein to yield the blank samples. Following a 1-h incubation at room temperature,[14] samples were scanned from 260 to 210 nm with the following instrument settings: 1.00 nm bandwidth, 0.5 nm data pitch, 50 nm/min scan rate, 4 s average time, 25 °C. One accumulation was acquired for each condition. The blank spectrum acquired for each high:low ratio was subtracted from the corresponding Tb^{III}−LanM spectrum, and $[\theta]_{222\ nm}$ was plotted vs free metal concentration.

Time-Resolved Luminescence for $K_{d,app}$ Determination on a Plate Reader. EDDS-buffered solutions of Tb^{III} were prepared as described above. Protein was added to the low and high Tb^{III}−EDDS solutions separately to a final concentration of 10 μM, and EDDS solutions were mixed at various high:low ratios. Following a 1-h incubation at room temperature, time-resolved luminescence emission was monitored from 400 to 700 nm on a BioTek Synergy H1 microplate reader in Greiner Cellstar 96-well half area μClear plates with the following instrument settings: time-resolved delay 50 μs, collection time 1000 μs, fixed excitation at 295 nm, emission 400−700 nm with 1 nm steps, gain of 120, and read speed delay 200 ms. Data points were corrected for the significant contribution from emission of the Tb^{III}−EDDS complex, determined by running matching samples in the absence of protein. Data were analyzed by

https://doi.org/10.1021/jacs.1c06360
J. Am. Chem. Soc. XXXX, XXX, XXX−XXX

averaging the fluorescence emission at 544−546 nm and plotting against $[Tb^{III}_{free}]$.

Luminescence Lifetimes for *q* Determination. Protein was diluted to 10 μM with 30 μM $TbCl_3$ in Buffer C. To make D_2O-containing samples, protein solutions (3 mL) were lyophilized overnight and resuspended in an equal volume of D_2O, the process was repeated, and then 10 μM protein in H_2O and 10 μM protein in D_2O were mixed in different proportions to achieve the percent D_2O concentrations desired (0−75%). Lifetime measurements were obtained on a PerkinElmer FL 6500 Fluorometer with the following parameters: data mode phosphorescence (short), excitation correction off, source mode pulse, flash count 1, flash power 120 kW, frequency 50 Hz, excitation wavelength 295 nm, excitation slit 5 nm, excitation filter air, emission wavelength 545 nm, emission slit 5 nm, emission filter air, PMT voltage 700 V, PMT gain auto, emission correction off, response time 0.5 s, delay time 0 μs, gate time 20 ms. Three independent trials were performed for each condition, and the $1/\tau$ values determined from the fitted curves were averaged and plotted against percent H_2O to determine $1/\tau(D_2O)$ from the y intercept of the line. The values of q were calculated using the method of Horrocks (eq 1),[34,49] where A = 5.0 ms, and a correction factor of −0.06 ms^{-1} was applied.[50]

$$q = A\left(\frac{1}{\tau(H_2O)} - \frac{1}{\tau(D_2O)}\right) \quad (1)$$

Stopped-Flow Fluorometry. Stopped-flow fluorometry measurements were carried out at 25 °C, maintained by a circulating water bath. One syringe contained a solution of 10 μM Trp-LanM and 30 μM $TbCl_3$, prepared in Chelex-treated Buffer C. Three equiv of Tb^{III} was used to minimize occupancy of EF4, adjacent to T41W; this stoichiometry is sufficient to fully (T41W) and nearly fully (T90W) saturate the proteins' Tb^{III}-dependent conformational changes (see Results). The contents of this syringe were mixed in a 1:1 ratio with solutions of EGTA (10, 5, 2.5, and 1.25 mM, in Chelex-treated Buffer C) in a second syringe. Data were acquired with the following parameters: 1 mm slit width, 2 mm path length, excitation at 295 nm, collecting 2000 data points over 120 s (T41W) or 200 s (T90W), and 12.5 μs sample period. Three shots were collected and averaged for each condition. Although a 450 nm long-pass filter was used, there was some residual Trp fluorescence in addition to the LRET signal in the emission channel. Curve fitting was performed in Origin 2018, fitted to either a single-exponential (T41W) or a double-exponential (T90W) decay.

Determination of Limits of Detection in Plate Reader Luminescence Assays. $TbCl_3$ stock solutions (10−50 μM) were made fresh each day in 20 mM acetate, 100 mM KCl, pH 5.0 (Buffer D). Protein samples were diluted to 1 or 10 μM in each of the following buffers: Buffer B (pH 7.0); Buffer D (pH 5.0); 20 mM acetate, 100 mM KCl, pH 4.0 (Buffer E); 20 mM ammonium formate, 100 mM KCl, pH 3.0 (Buffer F); and 20 mM ammonium formate, 100 mM KCl, pH 2.0 (Buffer G). Time-resolved luminescence emission was monitored from 400 to 700 nm (1 nm increments) in Greiner BioOne 96-well white flat-bottom Lumitrac plates with the following instrument settings: time-resolved delay 200 μs, collection time 1000 μs, fixed excitation at 280 nm, gain of 140, and read speed delay 100 ms. Full luminescence intensity was reached within the time between sample mixing and the first reading (~15 min). A blank containing buffer and Tb^{III} was subtracted from each corresponding spectrum prior to data analysis. Data were analyzed by averaging the emission at 544−546 nm from three independent replicates and plotting against Tb^{III} concentration (0.8−35.8 ppb, or 5−225 nM). Limits of detection were calculated from the slope (m) of the regression line (Origin 2018) and the standard deviation (s) of the sample with the lowest Tb^{III} concentration that displayed a peak across the entire pH range (2.4 ppb for T90W, or 15.9 ppb for T41W), according to eq 2. Limits of quantification were calculated by multiplying the LOD by 10/3.

$$\mathrm{LOD} = \frac{3s}{m} \quad (2)$$

Quantification of Tb^{III} in AMD Using T90W-LanM. Time-resolved luminescence emission was monitored from 400 to 650 nm in Greiner BioOne 96-well white flat-bottom Lumitrac plates with the same instrument settings as above. The sample volume was 200 μL. Using these settings, there was no significant emission from the AMD in the blank sample (without protein). For terbium detection, T90W-LanM was added to a concentration of 10 μM from a 1 mM stock in Buffer A. Addition of the protein did not significantly affect the pH of the AMD. Tb^{III} concentration was determined by averaging the emission at 544−546 nm. Full luminescence intensity was reached within the time between sample mixing and the first reading (~15 min). To enable Tb quantification, a standard curve was generated by mixing the same volumes of AMD and protein as above but with 0.4−2 μL of 2.5 ppm Tb^{III} in Buffer D added to yield 5−25 ppb Tb^{III}. The data with 0, 5, 10, 15, 20, and 25 ppb Tb^{III} added were fitted to a regression line, and the emission of the sample without Tb^{III} added was divided by the slope of the line, yielding the estimated Tb^{III} concentration.

RESULTS AND DISCUSSION

Determination of Optimal Trp Insertion Points in LanM. LanM possesses no Trp residues natively, facilitating our strategy to site-specifically probe metal binding using sensitized luminescence. On the basis of the NMR solution structure of Y^{III}-bound LanM,[18] we selected three positions in EF3—N87 (4th position), T90 (7th position), and K94 (11th position)—for Trp substitution and preliminary assays of energy transfer efficiency. We hypothesized that these substitutions would minimally interfere with metal ion binding yet also be sufficiently close to the Tb^{III} ion to yield a robust LRET signal. These variants were screened by stoichiometric Tb^{III} titrations (pH 7.2), exciting the Trp at 280 nm and monitoring in-growth of the luminescence spectrum of Tb^{III}, in particular, the most intense feature at ~545 nm, corresponding to the $^5D_4 \rightarrow {}^7F_4$ transition (Figure S2). In the case of N87W and K94W, Trp emission increased with addition of Tb^{III}, indicative of a change in environment of the fluorophore, presumably associated with the metal-induced conformational change. However, LRET was weak in these variants. Meanwhile, T90W showed the expected quenching of the Trp emission accompanied by strong Tb^{III} emission. Slight differences in the Tb^{III} binding stoichiometry were observed with these variants. Three equiv of Tb^{III} was sufficient to maximize Trp response and LRET signal for K94W but not other variants (4 equiv); by comparison, wild-type LanM binds 3 equiv of REEs with high affinity.[14] Therefore, K94W may introduce the least perturbation into EF3, but it gives a poor LRET signal. As a result, these preliminary studies suggested that the seventh position Thr residue was the most promising position for Trp substitution from the perspective of LRET efficiency. This result is consistent with characterization of other Trp-substituted EF-hand proteins including calmodulin[29] and synthetic Tb^{III} binding peptides[51] including LBTs.[44] Therefore, the seventh positions of the other three EF hands were substituted with Trp (T41W, T65W, T114W). All of these constructs exhibited robust sensitized Tb^{III} emission (Figure S3), whereas significant sensitized Eu^{III} emission was not observed, similar to other protein systems[49] (Figure S4). Presumably, the response of T114W (EF4) reflects energy transfer to the Tb^{III} bound in EF1.

The Trp-substituted LanM variants (Trp-LanMs) were evaluated by CD spectroscopy to determine whether the Trp

https://doi.org/10.1021/jacs.1c06360
J. Am. Chem. Soc. XXXX, XXX, XXX−XXX

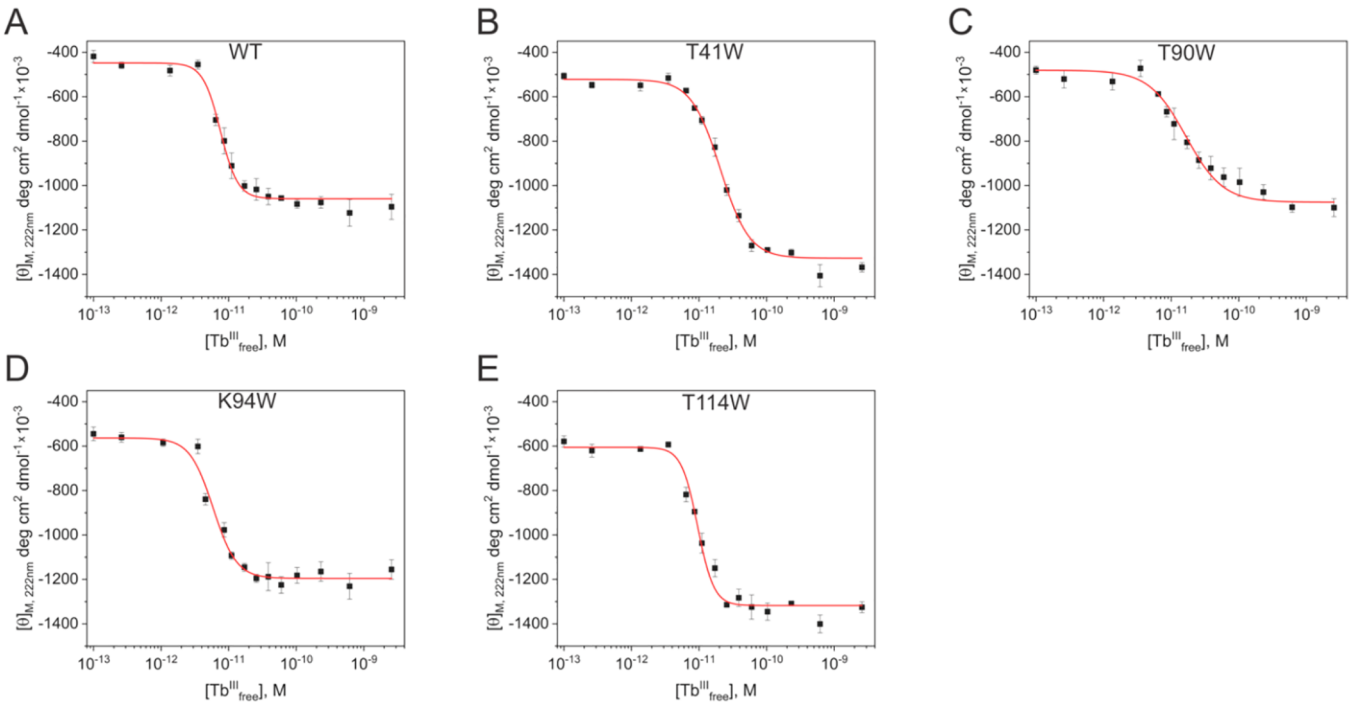

Figure 2. Determination of apparent K_d values for Tb^{III}–LanM complexes by CD spectroscopy for 15 μM (A) wild type, (B) T41W, (C) T90W, (D) K94W, and (E) T114W. $[\theta]_{222\ nm}$ was monitored at various EDDS-buffered free Tb^{III} ion concentrations, and data were fitted to the Hill equation to determine $K_{d,app}$ and n. Values from the fits are shown in Table 1. Mean ± SD for each point from triplicate measurements are displayed.

residue affected the apparent dissociation constant ($K_{d,app}$) and magnitude of the Tb^{III}-induced conformational change. All variants exhibited the same overall conformational change as wild-type LanM (~2.5–3-fold increase in the molar ellipticity at 222 nm, indicating increased helicity in the presence of Tb^{III} ions) with the notable exception of the EF2 insertion, T65W, which displays less helicity in the apoprotein as well as a nearly completely disrupted conformational response (Figure S5). As a result of the substantial perturbation introduced by the Trp residue in EF2, this site was not directly probed further, although T90W in EF3 does appear to report on metal binding to EF2 as well (vide infra). Disruptive effects resulting from substitution of Trp residues at the EF-hand seventh position have been observed previously for some Ca^{II} binding EF-hand proteins.[52] The other variants displayed full conformational response to 3 equiv of Tb^{III} with the exception of N87W and T90W, which required 4 equiv of Tb^{III}, similar to the fluorescence result (Figure S2).

$K_{d,app}$ values were determined for the Tb^{III}-bound Trp variants in comparison to wt LanM (Figure 2, Table 1). The substitutions most distal to metal binding sites (K94W in EF3 and T114W in EF4, which does not bind a metal under these conditions) displayed $K_{d,app}$ values and Hill coefficients (n) very similar to wt LanM. T41W (EF1) displayed a slight increase in $K_{d,app}$. By contrast, T90W was disruptive, appearing to break the conformational response into two phases with $K_{d,app}$ values of ~10 and ~100 pM; however, two-phase fits did not converge well, so the single-phase fit is reported here. Therefore, T41W and T114W are both suitable probes of metal binding to EF1, and K94W is the least disruptive probe for EF3, although its very weak LRET intensity could limit some experiments. The observation that T65W and (to a lesser extent) T90W, which are both at the interface of EF2 and EF3 (Figure 1), are the most disruptive substitutions also provides

Table 1. Apparent K_d Values and Hill Coefficients (n) for Trp-LanMs Determined using CD Spectroscopy (Figure 2) and Luminescence Methods (Figure S6) and Monitored at Various EDDS-Buffered Free Tb^{III} Ion Concentrations[a]

	circular dichroism titrations		luminescence titrations	
construct	$K_{d,app}$ (pM)	n	$K_{d,app}$ (pM)	n
WT	7.3 ± 0.9[b]	2.2 ± 0.5	NA[c]	NA[c]
T41W	22 ± 1	1.9 ± 0.2	42 ± 3	1.3 ± 0.1
T90W	17 ± 3	1.3 ± 0.2	66 ± 8	0.8 ± 0.1
K94W	6.1 ± 0.6	2.7 ± 0.5	6.2 ± 2.9	2.2 ± 0.6
T114W[d]	10 ± 1	2.1 ± 0.4	15 ± 1	1.5 ± 0.2

[a]Uncertainties represent mean ± SD for 3 independent experiments. [b]Note that the $K_{d,app}$ value for untagged wt LanM determined here is slightly lower (7.3 pM) than that for the C-terminally His-tagged protein initially characterized (21 pM); we have shown that the C-terminal tag slightly increases $K_{d,app}$ values.[14] All studies herein use untagged proteins. [c]NA: not applicable. [d]T114W appears to report on metal binding to EF1, although its position is within EF4 (see Figure 1D for residue positions within the EF hands).

important insights into LanM function. First, the failure of T65W-LanM to adopt the full helical structure of the wt protein suggests that EF2 is particularly critical for LanM's conformational change. Second, communication between EF2 and EF3 appears to be important for maintaining high Tb^{III} affinity overall, as suggested by characterization of T90W.

Time-Resolved Luminescence Elucidates Cooperative Linkages between LanM's EF Hands. Having characterized the overall conformational responses of the Trp-LanM variants, we next exploited the long-lived luminescence of Tb^{III} (Figure 3A) using time-resolved detection to probe the individual binding site(s) in the vicinity of each Trp residue. We reasoned that comparison of each of the extracted $K_{d,app}$ values and

https://doi.org/10.1021/jacs.1c06360
J. Am. Chem. Soc. XXXX, XXX, XXX−XXX

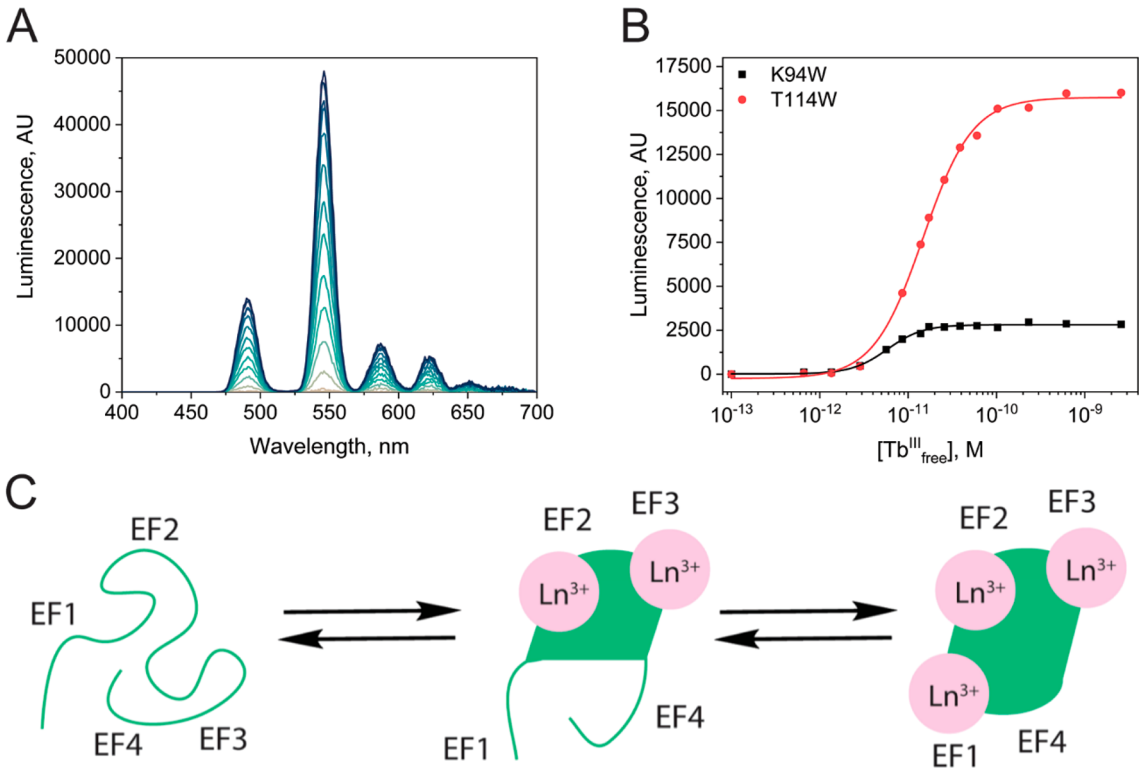

Figure 3. Using Tb^{III} LRET to probe metal binding order in LanM. (A) Representative LRET spectra from Tb^{III}-EDDS-buffered titration of T41W LanM. (B) Overlay of representative K94W and T114W LRET curves after subtraction of solutions containing the same Tb^{III} and EDDS concentrations but without protein. Data were analyzed by averaging the luminescence signal at 544−546 nm plotted against $[Tb^{III}_{free}]$ and fitted to the Hill equation. (C) Model for the order of Ln^{III} ion binding to LanM as proposed based on comparison of CD and LRET Tb^{III} binding data for wt and Trp-LanM variants.

cooperativities (Hill coefficient, n) to the CD-derived values for the whole protein could enable deduction of the order of metal binding and connectivity between the three EF-hand binding sites.

Overall, T41W showed the largest LRET response, followed by T90W and T114W, with K94W showing the smallest (Figure S6), although all four constructs studied had sufficient responses to allow determination of apparent K_d values and Hill coefficients. T41W and T114W, which both report on Tb^{III} binding to EF1 (Figure 1), exhibited lower Hill coefficients and slightly higher $K_{d,app}$ values as determined by the LRET titrations compared to the CD titrations (Table 1). Because the CD titration of T114W is least perturbed from wt values, this variant likely serves as the better reporter of EF1 binding; therefore, the $K_{d,app}$ of EF1 is likely ∼15 pM (the value derived from LRET), slightly weaker than the main response. These observations suggest that metal binding to EF1 does not account for the main conformational response of LanM (i.e., it is the weakly cooperative second phase). However, because the Hill coefficients associated with the probes of EF1 binding are not exactly equal to 1, it is possible that metal binding to EF1 is slightly influenced by the main binding event (vide infra), perhaps via the helical connectivity between EF1 and EF2 (Figure S1).

Consistent with the CD titrations, T90W is clearly a disruptive position for Trp placement within EF3, as revealed by a Hill coefficient $n \approx 1$, indicating a lack of cooperativity, and a high $K_{d,app}$ as compared to wt. Interestingly, the $K_{d,app}$ value derived from the LRET data approximately corresponds to the apparent second phase in the CD titrations with $K_{d,app} \approx$ 100 pM. These large perturbations mean that we cannot draw conclusions about the cooperativity of metal binding using this variant. Therefore, the K94W variant, which displayed fully wt behavior in CD titrations, was instead used to investigate Tb^{III} binding to EF3. Although the LRET intensities observed with this variant were very low (Figure 3B, Figure S2C), the apparent K_d was identical with the values determined by CD for this variant as well as for the wt, suggesting that EF3 is involved in LanM's primary metal-induced conformational change. Despite the fact that this Trp residue is predicted to be much closer to the Tb^{III} bound in EF3 (∼9 Å) than to any other EF hand (e.g., ∼18 Å from EF2) and therefore likely only reports on EF3, the Hill coefficient was ∼2, indicating positive cooperativity between Tb^{III} binding to EF3 and to at least one other EF hand. Because EF1 is ruled out from the above considerations, EF3 must be communicating with EF2, supporting the conclusion from the previous section.

Together, these data support the model for metal binding and conformational change presented in Figure 3C. Metal binding events in EF2 and EF3 display strong positive cooperativity and together are responsible for the major conformational change in the protein, accounting for ∼2/3 of its helical content. Metal binding to EF1 is slightly weaker and only weakly connected to binding at the other sites, and it is responsible for the remaining one-third of the protein's helical content.

Luminescence Lifetimes To Investigate Coordinated Solvent. Another critical aspect of understanding LanM's function is the structure of the metal binding sites. Our determination of the NMR structure of Y^{III}-bound LanM was

https://doi.org/10.1021/jacs.1c06360
J. Am. Chem. Soc. XXXX, XXX, XXX−XXX

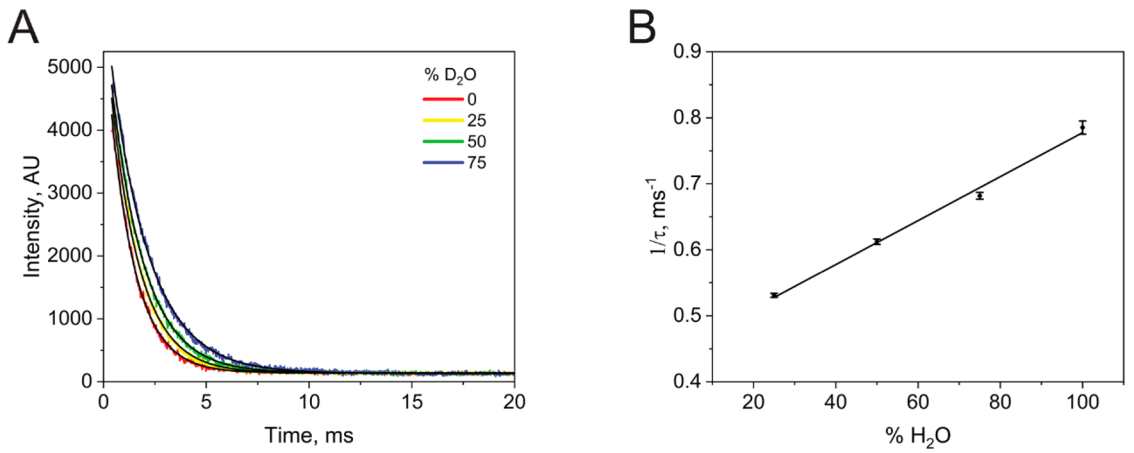

Figure 4. Determination of the luminescence lifetime of Tb^{III} bound to EF1. (A) T41W-LanM luminescence decay curves in 0%, 25%, 50%, and 75% D_2O. Data from each curve (carried out in triplicate) were fitted to a single-exponential decay. (B) Linear dependence of the decay time constant at different mole fractions of D_2O. $\tau(D_2O)$ was determined from the y intercept.

unable to determine whether protein residues saturated the metal binding sites or whether solvent molecules filled part of the coordination spheres. This information can be obtained from the lifetime of the Tb^{III} excited state, which is sensitive to the presence of coordinated water molecules due to the radiationless decay of the excited state via O−H vibrations.[26,34] Because this decay pathway is suppressed in D_2O, the empirical relationship between the difference in decay rate constants (τ^{-1}) in the presence of H_2O and D_2O has been shown to yield the approximate number of coordinated water molecules (q).[34,50] Therefore, we probed LanM using this method utilizing the T41W, T90W, and K94W variants because of their representation of both pairs of EF hands. In all cases, the decays of the luminescence signals could be fitted to single exponentials (Figure 4 for T41W, Figure S7 for T90W, and Figure S8 for K94W). By varying the mole fraction of D_2O in the protein solution, the q values determined are 2.0 ± 0.1 for T41W, 1.4 ± 0.1 for T90W, and 2.6 ± 0.1 for K94W. Because of the perturbations introduced by the T90W substitution, we suggest that the K94W data are more likely to represent solvent coordination for the native EF3. It is also possible that the T90W data reflect contributions from both EF2 and EF3. Nevertheless, the data suggest that both EF1 and EF3 metal binding sites coordinate roughly two solvent molecules. The presence of water molecules coordinated to Tb^{III} or Eu^{III} ions used to probe metal binding in Ca^{II} binding EF hands proteins is common;[26] for example, luminescence studies have found q = 2 for Ln^{III}-bound metal sites in calmodulin[53] and q = 1 in parvalbumin.[54] Therefore, despite the protein's unique affinity and selectivity for lanthanides, lanmodulin's metal sites are rather typical among EF-hand proteins with regard to solvent coordination. This result raises the question of whether the additional, conserved carboxylate residues at position 9 of LanM's EF hands are in fact coordinated, as originally proposed, or perhaps involved in hydrogen bonding with a coordinated water molecule, as residues at this position sometimes are in Ca^{II} binding EF hands.[16] In addition, because the presence of coordinated solvent would be expected to increase the rate constant for metal ion dissociation, we next sought to use stopped-flow spectrofluorometry to probe the kinetics of the system in order to better understand LanM's metal selectivity.

Probing the Kinetics of Tb^{III} Binding Using Stopped-Flow Spectrofluorometry. LanM's remarkable affinity for lanthanides may be explained by a faster rate of metal association, slower rate of metal dissociation, or both, relative to other EF-hand proteins. The large luminescence changes associated with Tb^{III} binding to the T41W and T90W LanM variants, despite the perturbations in apparent K_d, allowed us to use stopped-flow fluorometry to investigate the kinetics of site-specific Tb^{III} dissociation from LanM. In these experiments, the Trp-LanM variants were preloaded with 3 equiv of Tb^{III} and rapidly mixed with solutions of ethylene glycol-bis(β-aminoethyl ether)-*N*,*N*,*N*′,*N*′-tetraacetic acid (EGTA) at four different concentrations, and decay of the fluorescence signal above 450 nm (primarily the Tb^{III} luminescence) was monitored. Plotting of the decay rate constants (k_{obs}) at each EGTA concentration and extrapolation of the line to zero EGTA enables estimation of the dissociation rate constant (k_{off}) in the absence of chelator (Figure 5). The T41W fluorescence decays could be fitted to single exponentials, resulting in a k_{off} of 0.033 ± 0.001 s^{-1}. By contrast, fitting the T90W decays to a single exponential did not yield acceptable residuals (Figure S9); fitting to two exponential phases was

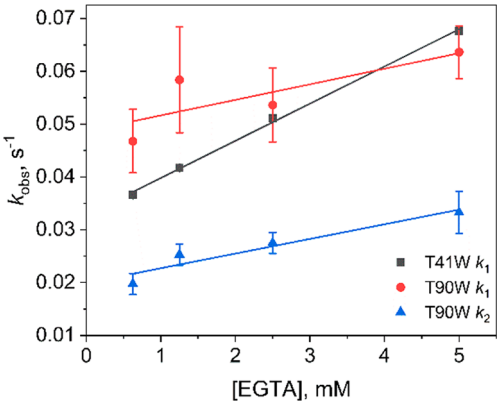

Figure 5. Determination of Tb^{III} dissociation kinetics by stopped-flow spectrofluorometry. Experimental curves were fitted to a single-exponential (T41W) or double-exponential (T90W) decay, and rate constants were plotted (mean ± SD, n = 3) against EGTA concentration. k_{off} values were determined from the y intercepts of the linear fits.

https://doi.org/10.1021/jacs.1c06360
J. Am. Chem. Soc. XXXX, XXX, XXX−XXX

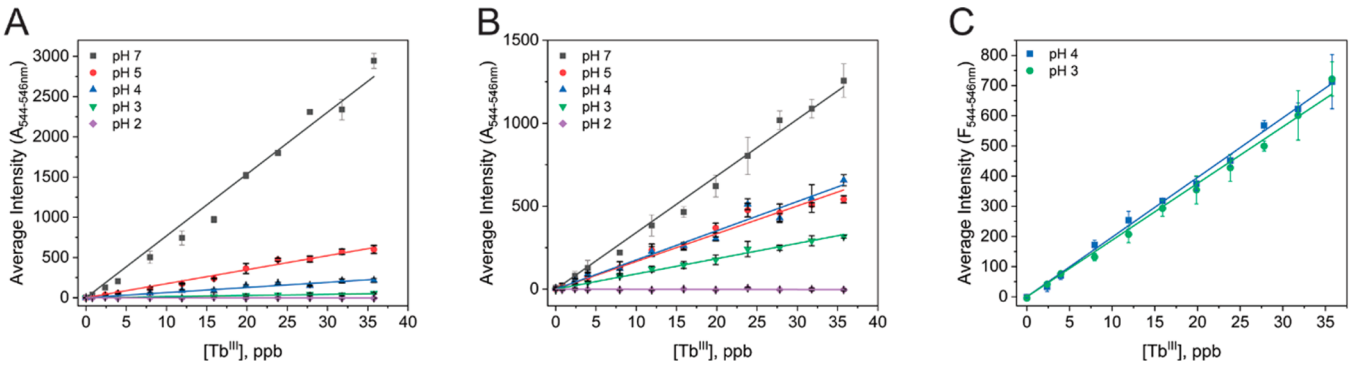

Figure 6. Calibration curves for Trp-LanM-sensitized Tb^{III} luminescence at the major peak ($F_{544-546\ nm}$) versus [Tb^{III}] (ppb) with (A) 1 μM T41W and (B) 1 μM T90W, from which LODs were determined. (C) Calibration curves for 10 μM T90W, pH 3 and 4. The similar slopes under these conditions (18.8 at pH 3, 19.8 at pH 4) suggest similar saturation of the protein at both pH values, which bracket the pH of the AMD sample analyzed below.

necessary, resulting in k_{off} values of 0.049 ± 0.005 and 0.020 ± 0.002 s^{-1} (Table S3). The requirement for two phases to fit the T90W data may reflect the position of this Trp residue between EF3 and EF2, allowing communication to each EF hand; the failure to distinguish a second phase in the luminescence decay experiments above may reflect either the lower signal-to-noise in the decay experiment or an identical q value for both metal binding sites. In support of the ability of Trp residues at the seventh position to communicate with both EF hands in the pair, the T114W (EF4) variant exhibits LRET when Tb^{III} is bound in EF1 (Figure S6, Table 1). Therefore, we suggest that the two phases report on metal dissociation from EF2 and EF3, respectively, but we are unable to assign each phase to a particular EF hand. We speculate that the faster k_{off} may be associated with EF3 based on the influence of T90W on apparent K_ds measured by CD and steady-state LRET (Table 1). Of course, such perturbations from introduction of Trp residues may mean that the true k_{off} values for the wt protein may be somewhat smaller than those determined here. Nevertheless, the data suggest that the three metal binding EF hands in LanM have relatively similar dissociation rate constants on the order of 0.02−0.05 s^{-1}.

Even though LanM exhibits several orders of magnitude higher affinities for Ln^{III} ions than most other EF-hand proteins, LanM's k_{off} values are within the typical range for Tb^{III} dissociation from the proteins in this family (e.g., 0.05 and 0.5 s^{-1} for parvalbumin[31] and 0.01 s^{-1} for galactose binding protein[32]). The similarity of these values may be accounted for by the similar numbers of coordinated solvent molecules, as determined above. From the k_{off} values and $K_{d,app}$ values (Table 1), both determined based on LRET, k_{on} was estimated to be ∼8 × 10^8 M^{-1} s^{-1} for T41W and 3−7 × 10^8 M^{-1} s^{-1} for T90W (in the case of T90W, a single $K_{d,app}$ value from the LRET titrations but two different k_{off} values prevents calculation of a single k_{on}). These rate constants are very close to the diffusion limit, which is on the order of 10^9−10^{10} M^{-1} s^{-1}.[55] Such rapid association kinetics may help to account for LanM's remarkable ability to selectively bind lanthanides even in very complex solutions with hundreds of millions-fold excess of competing metal ions.[15] In future work, it will be intriguing to probe the k_{on} and k_{off} values for non-REEs. Therefore, the optimization of LanM's k_{on} values for lanthanide binding appears to be a key feature of the protein's metal recognition, whereas its dissociation rates are rather typical among EF-hand proteins. However, control of k_{off} may still be important; the observation that k_{on} is near-optimal even for Tb^{III}, whereas LanM has even higher affinity for the early Ln^{III} ions, suggests that k_{off} differences may govern LanM's selectivity within the lanthanide series, which will be the subject of future work.

Trp-LanMs Exhibit Low Limits of Detection over a Wide pH Range. Whereas experiments with Trp-LanMs to characterize mechanism, structure, and kinetics of LanM were carried out at pH 7.2, potential broader application of these proteins as sensors would require responsiveness under a range of conditions, particularly in the presence of other metal contaminants and at low pH. Although LanM can selectively and quantitatively extract REEs from low-grade feedstocks containing only 30 ppm (∼200 μM) total REEs,[15] environmental samples such as AMD typically harbor much lower concentrations, <1 ppm REEs, and Tb^{III} at only low parts per billion levels.[6] Meanwhile, both these applications and monitoring of industrial processes necessitate robust performance at lower pHs than our previous LaMP1 sensor[47] could provide. With an eye toward these applications, we first determined the pH dependence and limits of detection (LODs) of Trp-LanM luminescence.

We again focused on the T41W and T90W variants, as they exhibited the greatest sensitized luminescence intensity of the Trp-LanM constructs characterized. Standard curves were generated with Tb^{III} concentrations ranging from 0.8 to 36 ppb and between pH 2 and pH 7 in the presence of 1 or 10 μM of each protein. Given the long luminescence lifetime observed (Figure 4), samples were detected in time-resolved luminescence mode on a plate reader. At pH 3−7, linear responses were observed for both proteins (Figure 6). Neither protein responded at pH 2. Because REEs have been shown to desorb from the protein at pH ≈ 2.5, this result reinforces that the observed luminescence signal is specific to interaction with LanM. Whereas at 1 μM, T90W-LanM exhibits a lower slope at pH 3 than at pH 4−5 (Figure 6B), increasing the concentration to 10 μM results in constant slopes at pH 3 and 4 (Figure 6C), suggesting that the metal is essentially fully bound to protein under the latter conditions. Interestingly, although T41W performed better than T90W at pH 7, its luminescence declined more quickly at lower pH values than that of T90W. Because wt LanM retains binding of 3 equiv of REEs even down to pH 3,[15] this decline is unlikely to result from metal dissociation. Instead, we note that the magnitude of the conformational response measured by CD decreases slightly at lower pH values.[15] Together, even though the

https://doi.org/10.1021/jacs.1c06360
J. Am. Chem. Soc. XXXX, XXX, XXX−XXX

Table 2. Limits of Detection (LODs) and Limits of Quantification (LOQs) for Tb^{III}, in ppb, of T41W and T90W LanM Variants, at pH 3−7, Using 1 or 10 μM Protein[a]

construct	pH 7	pH 5	pH 4	pH 3
		LOD (ppb)		
T41W-LanM	1.52 ± 0.03	0.38 ± 0.02	10.6 ± 0.6	19 ± 3
T90W-LanM (1 μM)	2.4 ± 0.1	3.2 ± 0.2	1.30 ± 0.03	4.8 ± 0.3
T90W-LanM (10 μM)	ND	ND	2.4 ± 0.1	0.78 ± 0.02
		LOQ (ppb)		
T41W-LanM	5.1 ± 0.1	1.3 ± 0.1	35 ± 2	62 ± 10
T90W-LanM (1 μM)	7.9 ± 0.4	10.6 ± 0.5	4.3 ± 0.1	16 ± 1
T90W-LanM (10 μM)	ND	ND	8.0 ± 0.3	2.6 ± 0.1

[a]Each number denotes the mean ± SD (n = 3). ND: not determined.

$K_{d,app}$ of EF1 is similar to that of EF2/3 at pH 7.2 as demonstrated by our LRET studies (Table 1), these results suggest that EF1 becomes more conformationally labile at lower pH, perhaps because it is paired with EF4, which does not bind metal ions tightly.

For comparison of Trp-LanM performance with other luminescence-based Tb^{III} sensors, LODs and limits of quantification (LOQs) were calculated as described in the Experimental Section. The LODs of the best-performing sensor at low pH, T90W, are below 5 ppb over the pH 3−7 range, even at 1 μM T90W (Table 2). Even at pH 3, our LOD values are similar to (or better than) the lowest values reported for other complexes, which are often reported at pH 7.[37,42] These results suggested that T90W-LanM might be robust enough to detect Tb^{III} even in challenging environmental samples.

Application to Quantification of Terbium in Acid Mine Drainage. In order to stringently challenge the affinity and selectivity of Trp-LanM and assess its potential for environmental monitoring, we tested the performance of the most promising construct, T90W-LanM, in acid mine drainage. AMD is effluent from active and abandoned mines by which natural processes lead to release of metals, including REEs, from ores. AMD is often enriched in the rarer and more valuable heavy REEs due to the mechanism of natural acid-based extraction processes.[6] The presence of the existing infrastructure required to treat AMD sites and mitigate their environmental impact prior to release of the AMD into natural waters has motivated investigation into the feasibility of extracting REEs from these sources in order to convert waste into revenue streams.[56−58] An estimated 770−3400 tonnes of REEs is potentially accessible per year from AMD in Pennsylvania and West Virginia (United States) alone;[57] for comparison, current domestic consumption of REEs is estimated at 13 000 tonnes per year.[38] A field-deployable sensor for specific REEs such as terbium or even a simpler lab procedure for analysis could enable more rapid assessments of the value of new sites for development for REE extraction as well as inexpensive in-line monitoring of extraction processes once implemented, compared to current ICP-MS or X-ray fluorescence elemental quantification methods.

We used a samples of AMD (pH 3.24) collected from the feed of an AMD treatment facility in Pennsylvania, United States.[6] Analysis of the sample using ICP-MS showed the presence of 300 ppm total metal ions, including high levels of potential interferents: 239 ppm (9.6 mM) Mg, 25 ppm (0.45 mM) Mn, 19 ppm (0.70 mM) Al, 12 ppm (0.41 mM) Si, and 1.5 ppm (22 μM) Zn (see Table S4 for full analysis). The sample also contained 280 ppb (2.3 μM) total REEs and only 3.3 ppb (21 nM) Tb^{III}. A sensor concentration of 1 μM did not yield a luminescence signal clearly above the background. Although LanM's slight preference for the more abundant early lanthanides may contribute partially to this result, the LODs for T90W-LanM at pH 3 (Table 2) suggest that the primary limitation under these conditions is that the pH of the AMD (3.2) is close to the apparent pK_a of the metal sites (~2.5−3),[15] and therefore, the K_d is on the same order as the protein concentration. Accordingly, and consistent with Table 2, when 10 μM T90W-LanM—a concentration far below the total metal concentration—was added, the Tb^{III} luminescence features at ~490 and ~545 nm were clearly visible above the background sample with no protein added (Figure 7A). Whereas the combination of the 100-fold excess of other REEs over terbium, 100 000-fold excess of non-REEs, and low pH would present a formidable challenge to most luminescence-based Tb^{III} detection methods, T90W-LanM's ability to detect Tb^{III} is consistent with LanM's high affinity for REEs and negligible binding of non-REEs, previously observed.[14,15]

Because components of the AMD matrix (other metal ions as well as anions) could affect quantification, a standard curve was generated in the AMD itself by adding 0−25 ppb Tb^{III} in the presence of 10 μM T90W-LanM (Figure 7B). Because the luminescence of the AMD in the absence of protein is negligible, dividing the intensity of the AMD sample without added Tb (33 ± 11) by the slope of the regression line (8.3) yields a Tb^{III} concentration of 4.0 ± 1.3 ppb (Figure 7C). This value, close to but above the limit of quantification at pH 3, is in excellent agreement with the value determined by ICP-MS, 3.3 ppb. Because the slope of the line is only 50% lower than those of the standard curves obtained in idealized Tb^{III} solutions at pH 3 and 4, we suggest that the LODs determined under these conditions may be limited more so by the sensitivity of the plate reader than by the affinity or selectivity of the protein. Using more sensitive detectors (e.g., a spectrofluorometer), lower LODs could conceivably be achieved. Therefore, T90W-LanM is an exceptionally sensitive sensor for Tb^{III}, applicable even in complex, environmental samples such as AMD.

The performance of Trp-LanM (and T90W-LanM specifically) in detecting Tb^{III} at low concentration even in complex media compares favorably with other luminescence-based sensors, both biomolecular and synthetic.[13,37] Perhaps most conceptually similar to Trp-LanM is the LBT, but its affinity for Tb^{III} is only 60 nM at pH 7[44] (or 3 nM for one site in the "double LBT" construct[59]). Because this affinity is 3−4 orders of magnitude lower than that of LanM, LBTs would not be expected to function at pH 3. Indeed, attempts to use LBTs for Tb^{III} binding and sensing at pH values below ~5−6 have been

https://doi.org/10.1021/jacs.1c06360
J. Am. Chem. Soc. XXXX, XXX, XXX−XXX

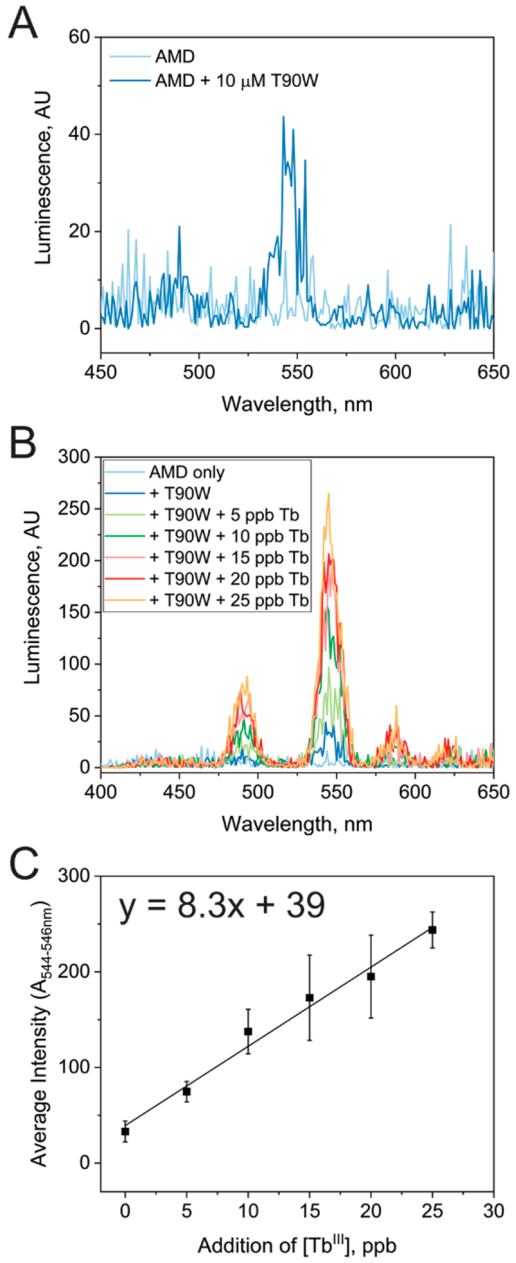

Figure 7. T90W-LanM quantifies Tb^{III} in AMD. (A) Luminescence spectra of AMD with and without 10 μM T90W-LanM. (B) Same as A but also including spectra upon addition of 5–25 ppb Tb^{III} for generation of a calibration curve. (C) Standard curve obtained from the data in B with the equation of the regression line used to quantify Tb^{III} in the AMD sample.

unsuccessful.[46] A cell-based sensor incorporating an LBT into a bacterial two-component system responds to as little as ~0.2 μM (30 ppb) Tb^{III} at neutral pH but also responds significantly to other metals (e.g., Ca^{II} at 50 μM) at concentrations that would be present in environmental samples (e.g., our AMD sample contains 3.11 ppm, or 78 μM, Ca).[60] Numerous synthetic luminescence-based sensors for lanthanides, including terbium, have been characterized with a wide range of detection limits.[37] Some of these sensors have been characterized in natural samples, although at higher pH values than AMD and spiked with Tb^{III}.[61,62] A particularly extensively explored approach in recent years utilizes MOFs, exhibiting better tolerance to lower pHs than LBTs and other sensors but also quenching from interactions with other ions due to low selectivity.[37,63] One of the most promising examples is a zinc–adeninate MOF for detection of several lanthanides (BioMOF-100), yielding an LOD for Tb^{III} of 90 ppb in neutral water.[41] Very recently, Crawford and co-workers characterized even more sensitive MOFs with LODs of 6 ppb Tb^{III} in neutral water. However, when this sensor was applied in an AMD sample containing ~1 ppb Tb^{III} at pH 3.4, the sample had to be spiked with 800 ppb (5 μM) Tb^{III} to be able to observe a signal.[42] By contrast, simply adding T90W-LanM directly to AMD detects and quantifies 3 ppb Tb^{III} present in AMD at pH 3.24 without any spiking. This comparison shows that the high affinity and selectivity of LanM for lanthanides provides a significant advantage over conventional REE sensitizer ligands, which (while they may have high affinity) usually do not have sufficient selectivity to work well in complex solutions like AMD. Indeed, to the best of our knowledge, our work represents the first time that Tb^{III} can be quantified at such low levels in AMD or a similar, low-pH environmental sample using a luminescence-based sensor.

CONCLUSION

Incorporation of Trp residues site specifically into LanM's metal binding sites not only provides insights into the protein's metal recognition but also yields a technology capable of specific detection of terbium, even in complex samples. This work establishes several key aspects of LanM function. First, our results point to EF2 and EF3 as being LanM's preferred metal binding sites and responsible for the cooperative binding phase. EF1 has slightly lower affinity but interestingly appears to be more destabilized at low pH values, even though metal binding is retained.[13,15] This result suggests that EF1 might be the most dispensable site for applications of LanM to REE extraction and separations. In addition, we suggest that LanM-bound Tb^{III} ions possess roughly two coordinated solvent molecules. The presence of these coordinated solvent molecules may explain our observation that LanM's association kinetics are extremely and uncommonly fast, perhaps minimizing the energetic penalty for dehydration upon metal binding.[64,65] Rapid kinetics may be useful for separations applications, whereas these results also suggest that it may be possible to mutate the protein to decrease metal dissociation rates for other applications. Furthermore, our work establishes that EF3, and particularly the T90W position, is an especially fruitful location for installation of sensitizers within the protein scaffold with acceptable perturbation of metal binding and strong responsiveness across a wide pH range. Of the variants tested here, T90W-LanM is optimal for terbium detection under a range of conditions; however, it is easy to imagine a pathway for further optimization and extension of the system. Other lanthanides can be detected besides terbium via their unique luminescence signatures, including other valuable REEs, such as Eu^{III}, Dy^{III}, Sm^{III}, and Nd^{III},[21,37] but Trp is not a suitable sensitizer for these elements nor is Trp ideal due to its ultraviolet excitation. Our results lay the groundwork for site-specific incorporation of other sensitizers into LanM that would allow sensitive detection of other lanthanides as well as even more sensitive detection of Tb^{III}.[66,67] In addition, because wt LanM favors early lanthanides, one can envision extension of this approach to LanM variants with distinct selectivity profiles that favor middle–late lanthanides[14] to further optimize detection. Increasing the overall lanthanide affinity of the protein would also be important for enabling metal

https://doi.org/10.1021/jacs.1c06360
J. Am. Chem. Soc. XXXX, XXX, XXX–XXX

quantification at the lowest pH values using lower protein concentration (Table 2). Finally, the related coordination chemistry of the trivalent actinides suggests that Trp-LanMs may also serve as efficient sensitizers for some of these elements, such as Cm^{III}.[68]

The robust performance of the Trp-LanM sensors builds on our prior work to detect total REEs at neutral pH[47] and to extract REEs under harsh conditions,[15] extending LanM's capabilities to facile detection of a specific REE in real environmental samples with potential extension to detection of other elements. Furthermore, the detection of terbium in a sample would indicate the likely presence of higher concentrations of other generally more abundant but also valuable rare earths, such as neodymium and dysprosium. The small quantities of protein required and the adaptability of this system to available luminescence detectors motivates further exploration and application of protein-based systems for rapid and inexpensive quantification of specific f elements in natural sources and in separation processes.

■ ASSOCIATED CONTENT

Supporting Information

The Supporting Information is available free of charge at https://pubs.acs.org/doi/10.1021/jacs.1c06360.

Supplemental tables (including primers and plasmids, kinetic parameters, and full ICP-MS analysis of the AMD sample) and figures (including additional CD, stopped-flow, and luminescence data) (PDF)

■ AUTHOR INFORMATION

Corresponding Author

Joseph A. Cotruvo, Jr. − *Department of Chemistry, The Pennsylvania State University, University Park, Pennsylvania 16802, United States;* orcid.org/0000-0003-4243-8257; Email: juc96@psu.edu

Authors

Emily R. Featherston − *Department of Chemistry, The Pennsylvania State University, University Park, Pennsylvania 16802, United States;* orcid.org/0000-0003-1338-6611

Edward J. Issertell − *Department of Chemistry, The Pennsylvania State University, University Park, Pennsylvania 16802, United States*

Complete contact information is available at: https://pubs.acs.org/10.1021/jacs.1c06360

Notes

The authors declare the following competing financial interest(s): J.A.C. and E.R.F. are listed as inventors on a patent application submitted by the Pennsylvania State University.

■ ACKNOWLEDGMENTS

We thank Prof. Sarma Pisupati and Prof. Mohammad Rezaee for providing the acid mine drainage samples used, Prof. Elizabeth Elacqua and Prof. Xin Zhang for use of their laboratories' spectrofluorometers, Profs. J. Martin Bollinger, Jr. and Carsten Krebs for use of their stopped-flow spectrophotometer, Dr. Rachelle Copeland for guidance on stopped-flow experiments, and Dr. Dongxiang Wang for assistance with ICP-MS. This research was supported by the National Science Foundation (CHE-1945015 to J.A.C.) and Penn State University (a Lab Bench to Commercialization grant and Louis Martarano Career Development Professorship to J.A.C. and an Erickson Discovery Grant to E.J.I.).

■ REFERENCES

(1) Cheisson, T.; Schelter, E. J. Rare earth elements: Mendeleev's bane, modern marvels. *Science* **2019**, *363*, 489−493.

(2) Xie, F.; Zhang, T. A.; Dreisinger, D.; Doyle, F. A critical review on solvent extraction of rare earths from aqueous solutions. *Miner. Eng.* **2014**, *56*, 10−28.

(3) Wang, L.; Huang, X.; Yu, Y.; Zhao, L.; Wang, C.; Feng, Z.; Cui, D.; Long, Z. Towards cleaner production of rare earth elements from bastnaesite in China. *J. Cleaner Prod.* **2017**, *165*, 231−242.

(4) Erickson, B. Rare-earth recovery: U.S. efforts to extract valuable elements from coal waste surge. *Chem. Eng. News* **2018**, *96* (28), 29−33.

(5) Binnemans, K.; Jones, P. T.; Blanpain, B.; Van Gerven, T.; Pontikes, Y. Towards zero-waste valorisation of rare-earth-containing industrial process residues: a critical review. *J. Cleaner Prod.* **2015**, *99*, 17−38.

(6) Vaziri Hassas, B.; Rezaee, M.; Pisupati, S. V. Precipitation of rare earth elements from acid mine drainage by CO_2 mineralization process. *Chem. Eng. J.* **2020**, *399*, 125716.

(7) Nakagawa, T.; Mitsui, R.; Tani, A.; Sasa, K.; Tashiro, S.; Iwama, T.; Hayakawa, T.; Kawai, K. A catalytic role of XoxF1 as La^{3+}-dependent methanol dehydrogenase in *Methylobacterium extorquens* strain AM1. *PLoS One* **2012**, *7*, e50480.

(8) Pol, A.; Barends, T. R. M.; Dietl, A.; Khadem, A. F.; Eygensteyn, J.; Jetten, M. S. M.; Op den Camp, H. J. M. Rare earth metals are essential for methanotrophic life in volcanic mudpots. *Environ. Microbiol.* **2014**, *16*, 255−264.

(9) Chistoserdova, L. Lanthanides: New life metals? *World J. Microbiol. Biotechnol.* **2016**, *32*, 138.

(10) Martinez-Gomez, N. C.; Vu, H. N.; Skovran, E. Lanthanide chemistry: From coordination in chemical complexes shaping our technology to coordination in enzymes shaping bacterial metabolism. *Inorg. Chem.* **2016**, *55*, 10083−10089.

(11) Daumann, L. Essential and ubiquitous: The emergence of lanthanide metallobiochemistry. *Angew. Chem., Int. Ed.* **2019**, *58*, 12795−12802.

(12) Cotruvo, J. A., Jr. The chemistry of lanthanides in biology: Recent discoveries, emerging principles, and technological applications. *ACS Cent. Sci.* **2019**, *5*, 1496−1506.

(13) Mattocks, J. A.; Cotruvo, J. A., Jr. Biological, biomolecular, and bio-inspired strategies for detection, extraction, and separations of lanthanides and actinides. *Chem. Soc. Rev.* **2020**, *49*, 8315−8334.

(14) Cotruvo, J. A., Jr.; Featherston, E. R.; Mattocks, J. A.; Ho, J. V.; Laremore, T. N. Lanmodulin: A highly selective lanthanide-binding protein from a lanthanide-utilizing bacterium. *J. Am. Chem. Soc.* **2018**, *140*, 15056−15061.

(15) Deblonde, G. J.-P.; Mattocks, J. A.; Park, D. M.; Reed, D. W.; Cotruvo, J. A., Jr.; Jiao, Y. Selective and efficient biomacromolecular extraction of rare-earth elements using lanmodulin. *Inorg. Chem.* **2020**, *59*, 11855−11867.

(16) Gifford, J. L.; Walsh, M. P.; Vogel, H. J. Structures and metal-ion-binding properties of the Ca^{2+}-binding helix-loop-helix EF-hand motifs. *Biochem. J.* **2007**, *405*, 199−221.

(17) Edington, S. C.; Gonzalez, A.; Middendorf, T. R.; Halling, D. B.; Aldrich, R. W.; Baiz, C. R. Coordination to lanthanide ions distorts binding site conformation in calmodulin. *Proc. Natl. Acad. Sci. U. S. A.* **2018**, *115*, E3126−E3134.

(18) Cook, E. C.; Featherston, E. R.; Showalter, S. A.; Cotruvo, J. A., Jr. Structural basis for rare earth element recognition by *Methylobacterium extorquens* lanmodulin. *Biochemistry* **2019**, *58*, 120−125.

(19) Bünzli, J.-C. G. On the design of highly luminescent lanthanide complexes. *Coord. Chem. Rev.* **2015**, *293*−*294*, 19−47.

(20) Selvin, P. R. Principles and biophysical applications of lanthanide-based probes. *Annu. Rev. Biophys. Biomol. Struct.* **2002**, *31*, 275−302.
(21) Bünzli, J.-C. G.; Piguet, C. Taking advantage of luminescent lanthanide ions. *Chem. Soc. Rev.* **2005**, *34*, 1048−1077.
(22) Mathieu, E.; Sipos, A.; Demeyere, E.; Phipps, D.; Sakaveli, D.; Borbas, K. E. Lanthanide-based tools for the investigation of cellular environments. *Chem. Commun.* **2018**, *54*, 10021−10035.
(23) Moore, E. G.; Samuel, A. P. S.; Raymond, K. N. From antenna to assay: Lessons learned in lanthanide luminescence. *Acc. Chem. Res.* **2009**, *42*, 542−552.
(24) Rajapakse, H. E.; Gahlaut, N.; Mohandessi, S.; Yu, D.; Turner, J. R.; Miller, L. W. Time-resolved luminescence resonance energy transfer imaging of protein−protein interactions in living cells. *Proc. Natl. Acad. Sci. U. S. A.* **2010**, *107*, 13582−13587.
(25) Brittain, H. G.; Richardson, F. S.; Martin, R. B. Terbium(III) emission as a probe of calcium(II) binding sites in proteins. *J. Am. Chem. Soc.* **1976**, *98*, 8255−8260.
(26) Horrocks, W. D. J. Luminescence spectroscopy. *Methods Enzymol.* **1993**, *226*, 495−538.
(27) Drake, S. K.; Lee, K. L.; Falke, J. J. Tuning the equilibrium ion affinity and selectivity of the EF-hand calcium binding motif: substitutions at the gateway position. *Biochemistry* **1996**, *35*, 6697−6705.
(28) Horrocks, W. D.; Holmquist, B.; Vallee, B. L. Energy transfer between terbium (III) and cobalt (II) in thermolysin: a new class of metal–metal distance probes. *Proc. Natl. Acad. Sci. U. S. A.* **1975**, *72*, 4764−4768.
(29) Kilhoffer, M. C.; Roberts, D. M.; Adibi, A. O.; Watterson, D. M.; Haiech, J. Investigation of the mechanism of calcium binding to calmodulin. Use of an isofunctional mutant with a tryptophan introduced by site-directed mutagenesis. *J. Biol. Chem.* **1988**, *263*, 17023−17029.
(30) Ye, Y.; Lee, H.-W.; Yang, W.; Shealy, S.; Yang, J. J. Probing site-specific calmodulin calcium and lanthanide affinity by grafting. *J. Am. Chem. Soc.* **2005**, *127*, 3743−3750.
(31) Breen, P. J.; Johnson, K. A.; Horrocks, W. D. Stopped-flow kinetic studies of metal ion dissociation or exchange in a tryptophan-containing parvalbumin. *Biochemistry* **1985**, *24*, 4997−5004.
(32) Renner, M.; Danielson, M. A.; Falke, J. J. Kinetic control of Ca(II) signaling: tuning the ion dissociation rates of EF-hand Ca(II) binding sites. *Proc. Natl. Acad. Sci. U. S. A.* **1993**, *90*, 6493−6497.
(33) Drake, S. K.; Falke, J. J. Kinetic tuning of the EF-hand calcium binding motif: The gateway residue independently adjusts (i) barrier height and (ii) equilibrium. *Biochemistry* **1996**, *35*, 1753−1760.
(34) Horrocks, W. D.; Sudnick, D. R. Lanthanide ion probes of structure in biology. Laser-induced luminescence decay constants provide a direct measure of the number of metal-coordinated water molecules. *J. Am. Chem. Soc.* **1979**, *101*, 334−340.
(35) Sindern, S. Analysis of rare earth elements in rock and mineral samples by ICP-MS and LA-ICP-MS. *Phys. Sci. Rev.* **2017**, *2*, 20160066.
(36) Young, K. E.; Evans, C. A.; Hodges, K. V.; Bleacher, J. E.; Graff, T. G. A review of the handheld X-ray fluorescence spectrometer as a tool for field geologic investigations on Earth and in planetary surface exploration. *Appl. Geochem.* **2016**, *72*, 77−87.
(37) Crawford, S. E.; Ohodnicki, P. R.; Baltrus, J. P. Materials for the photoluminescent sensing of rare earth elements: challenges and opportunities. *J. Mater. Chem. C* **2020**, *8*, 7975−8006.
(38) U.S.G.S. Mineral Commodity Summary-Rare Earths; https://www.usgs.gov/centers/nmic/rare-earths-statistics-and-information (accessed 2021−05−29).
(39) Deng, G. Terbium glows green. *Nat. Chem.* **2018**, *10*, 110−110.
(40) U.S. Department of Energy, Critical Materials Strategy, Dec 2011; https://www.energy.gov/sites/prod/files/DOE_CMS2011_FINAL_Full.pdf (accessed 2021−04−17).
(41) Crawford, S. E.; Gan, X. Y.; Lemaire, P. C. K.; Millstone, J. E.; Baltrus, J. P.; Ohodnicki, P. R. Zinc-adeninate metal−organic framework: A versatile photoluminescent sensor for rare earth elements in aqueous systems. *ACS Sensors* **2019**, *4*, 1986−1991.
(42) Crawford, S. E.; Ellis, J. E.; Ohodnicki, P. R.; Baltrus, J. P. Influence of the anionic zinc-adeninate metal−organic framework structure on the luminescent detection of rare earth ions in aqueous streams. *ACS Appl. Mater. Interfaces* **2021**, *13*, 7268−7277.
(43) Franz, K. J.; Nitz, M.; Imperiali, B. Lanthanide-binding tags as versatile protein coexpression probes. *ChemBioChem* **2003**, *4*, 265−271.
(44) Nitz, M.; Sherawat, M.; Franz, K. J.; Peisach, E.; Allen, K. N.; Imperiali, B. Structural origin of the high affinity of a chemically evolved lanthanide-binding peptide. *Angew. Chem., Int. Ed.* **2004**, *43*, 3682−3685.
(45) Bonnet, C. S.; Devocelle, M.; Gunnlaugsson, T. Luminescent lanthanide-binding-peptides: sensitising the excited states of Eu(III) and Tb(III) with a 1,8-naphthalimide-based antenna. *Org. Biomol. Chem.* **2012**, *10*, 126−133.
(46) Park, D. M.; Reed, D. W.; Yung, M. C.; Eslamimanesh, A.; Lencka, M. M.; Anderko, A.; Fujita, Y.; Riman, R. E.; Navrotsky, A.; Jiao, Y. Bioadsorption of rare earth elements through cell surface display of lanthanide binding tags. *Environ. Sci. Technol.* **2016**, *50*, 2735−2742.
(47) Mattocks, J. A.; Ho, J. V.; Cotruvo, J. A., Jr. A selective, protein-based fluorescent sensor with picomolar affinity for rare earth elements. *J. Am. Chem. Soc.* **2019**, *141*, 2857−2861.
(48) Featherston, E. R.; Mattocks, J. A.; Tirsch, J. L.; Cotruvo, J. A., Jr. Heterologous expression, purification, and characterization of proteins in the lanthanome. *Methods Enzymol.* **2021**, *650*, 119−157.
(49) Horrocks, W. D.; Sudnick, D. R. Lanthanide ion luminescence probes of the structure of biological macromolecules. *Acc. Chem. Res.* **1981**, *14*, 384−392.
(50) Beeby, A.; Clarkson, I. M.; Dickins, R. S.; Faulkner, S.; Parker, D.; Royle, L.; de Sousa, A. S.; Williams, J. A. G.; Woods, M. Non-radiative deactivation of the excited states of europium, terbium and ytterbium complexes by proximate energy-matched OH, NH and CH oscillators: an improved luminescence method for establishing solution hydration states. *J. Chem. Soc., Perkin Trans. 2* **1999**, 493−504.
(51) MacManus, J. P.; Hogue, C. W.; Marsden, B. J.; Sikorska, M.; Szabo, A. G. Terbium luminescence in synthetic peptide loops from calcium-binding proteins with different energy donors. *J. Biol. Chem.* **1990**, *265*, 10358−10366.
(52) Edington, S. C.; Halling, D. B.; Bennett, S. M.; Middendorf, T. R.; Aldrich, R. W.; Baiz, C. R. Non-additive effects of binding site mutations in calmodulin. *Biochemistry* **2019**, *58*, 2730−2739.
(53) Bruno, J.; Horrocks, W. D.; Zauhar, R. J. Europium(III) luminescence and tyrosine to terbium(III) energy-transfer studies of invertebrate (octopus) calmodulin. *Biochemistry* **1992**, *31*, 7016−7026.
(54) Rhee, M.-J.; Sudnick, D. R.; Arkle, V. K.; Horrocks, W. D. Lanthanide ion luminescence probes. Characterization of metal ion binding sites and intermetal energy transfer distance measurements in calcium-binding proteins. 1. Parvalbumin. *Biochemistry* **1981**, *20*, 3328−3334.
(55) Chou, K. C.; Zhou, G. P. Role of the protein outside active site on the diffusion-controlled reaction of enzymes. *J. Am. Chem. Soc.* **1982**, *104*, 1409−1413.
(56) Ayora, C.; Macías, F.; Torres, E.; Lozano, A.; Carrero, S.; Nieto, J.-M.; Pérez-López, R.; Fernández-Martínez, A.; Castillo-Michel, H. Recovery of rare earth elements and yttrium from passive-remediation systems of acid mine drainage. *Environ. Sci. Technol.* **2016**, *50*, 8255−8262.
(57) Vass, C. R.; Noble, A.; Ziemkiewicz, P. F. The occurrence and concentration of rare earth elements in acid mine drainage and treatment by-products: Part 1—Initial survey of the Northern Appalachian Coal Basin. *Mining Metall. Explor.* **2019**, *36*, 903−916.
(58) Zhang, W.; Noble, A.; Yang, X.; Honaker, R. A comprehensive review of rare earth elements recovery from coal-related materials. *Minerals* **2020**, *10*, 451.

https://doi.org/10.1021/jacs.1c06360
J. Am. Chem. Soc. XXXX, XXX, XXX−XXX

(59) Martin, L. J.; Hähnke, M. J.; Nitz, M.; Wöhnert, J.; Silvaggi, N. R.; Allen, K. N.; Schwalbe, H.; Imperiali, B. Double-lanthanide-binding tags: Design, photophysical properties, and NMR applications. *J. Am. Chem. Soc.* **2007**, *129*, 7106−7113.
(60) Liang, H.; Deng, X.; Bosscher, M.; Ji, Q.; Jensen, M. P.; He, C. Engineering bacterial two-component system PmrA/PmrB to sense lanthanide ions. *J. Am. Chem. Soc.* **2013**, *135*, 2037−2039.
(61) Vaněk, J.; Lubal, P.; Ševčíková, R.; Polášek, M.; Hermann, P. Mono(pyridine-N-oxide) analog of DOTA as a suitable organic reagent for a sensitive and selective fluorimetric determination of Ln(III) ions. *J. Lumin.* **2012**, *132*, 2030−2035.
(62) Chen, Q.; Zuo, J.; He, X.; Mo, X.; Tong, P.; Zhang, L. Enhanced fluorescence of terbium with thiabendazole and application in determining trace amounts of terbium and thiabendazole. *Talanta* **2017**, *162*, 540−546.
(63) An, J.; Shade, C. M.; Chengelis-Czegan, D. A.; Petoud, S.; Rosi, N. L. Zinc-adeninate metal−organic framework for aqueous encapsulation and sensitization of near-infrared and visible emitting lanthanide cations. *J. Am. Chem. Soc.* **2011**, *133*, 1220−1223.
(64) Dudev, T.; Lim, C. Principles governing Mg, Ca, and Zn binding and selectivity in proteins. *Chem. Rev.* **2003**, *103*, 773−788.
(65) Dudev, T.; Lim, C. Competition among metal ions for protein binding sites: Determinants of metal ion selectivity in proteins. *Chem. Rev.* **2014**, *114*, 538−556.
(66) Reynolds, A. M.; Sculimbrene, B. R.; Imperiali, B. Lanthanide-binding tags with unnatural amino acids: Sensitizing Tb^{3+} and Eu^{3+} luminescence at longer wavelengths. *Bioconjugate Chem.* **2008**, *19*, 588−591.
(67) Cho, U.; Chen, J. K. Lanthanide-based optical probes of biological systems. *Cell Chem. Biol.* **2020**, *27*, 921−936.
(68) Sturzbecher-Hoehne, M.; Goujon, C.; Deblonde, G. J. P.; Mason, A. B.; Abergel, R. J. Sensitizing curium luminescence through an antenna protein to investigate biological actinide transport mechanisms. *J. Am. Chem. Soc.* **2013**, *135*, 2676−2683.

https://doi.org/10.1021/jacs.1c06360
J. Am. Chem. Soc. XXXX, XXX, XXX−XXX